Compact Space-Multimode Diversity Stacked Circular Microstrip Antenna Array for 802.11n MIMO-OFDM WLANs

Alper Öcalan[#1], Asuman Savaşçıhabeş[*1], İbrahim Görgeç[#2], Özgür Ertuğ[*2], Erdem Yazgan[#3]

[*]*Gazi University, EEE Dept., Telecommunications and Signal Processing Laboratory (TESLAB), Turkey*

[1]asavascihabes@gazi.edu.tr, [2]ertug@gazi.edu.tr

[#]*Hacettepe University, EEE Dept., Turkey*

[1]alper.ocalan@turktelekom.com.tr, [2]igorgec@aselsan.com.tr, [3]yazgan@hacettepe.edu.tr

Abstract — **The support of MIMO communication in OFDM-WLAN systems conforming to IEEE 802.11n standard requires the design and use of compact antennas and arrays with low correlation ports. In this paper, the design and analysis of a compact space-multimode diversity provisioning stacked circular microstrip patch uniform linear antenna array (SCP-ULA) for MIMO-OFDM WLAN systems and the associated spatial and modal correlation, ergodic spectral efficiency and compactness gains with respect to dipole (DP-ULA) and circular microstrip patch uniform linear arrays (CP-ULA) with dominant-mode operation are presented.**

I.INTRODUCTION

In the concurrent and next-generation communication systems, the spectral efficiency and transmission quality can be vastly enhanced by multiple-input multiple-output (MIMO) communication techniques [1]. In communication systems employing MIMO spatial-multiplexing, higher data rates can be achieved when there are a large number of scatterers between the transmit and receive antennas i.e. rich-scattering environment. However, the spatial correlation between transmit and receive antenna ports that is dependent on antenna-specific parameters such as the radiation patterns, the distance between the antenna elements as well as the channel characteristics such as unfavourable spatial distribution of scatterers and angular spread severely degrades the capacity and quality achievable by MIMO spatial-multiplexing systems.

The space consumption of MIMO antennas is especially vital in applications such as access points, modems and end-user terminal equipments (laptops, PDAs etc.) of WLAN and WIMAX systems. When regularly spaced antenna elements are used in MIMO systems, the correlation between the antenna elements in a space diversity system and hence the channel capacity and transmission quality are dependent on the distance between antenna array elements, the number of antenna elements and the array geometry. However, due to the physical constraints and the concerns on ergonomics and aesthetics, the distance between antenna elements in practice can not be extended beyond a certain level which limits the use of space-only diversity MIMO spatial-multiplexing systems to achieve the desired spectral efficiencies and transmission qualities. As an alternative solution to achieve compactness in MIMO systems, the use of pattern diversity [2,3], multimode diversity [4,5], and polarization diversity [6,7] techniques in conjunction with space diversity are proposed in the literature.

Besides polarization diversity that is well-known, multimode and pattern diversity techniques that are less addressed in antenna engineering community are achieved by using higher-order mode generation in antenna structures and in general microstrip, biconical, helical, spiral, sinus and log-periodic antenna structures are amenable to higher-order mode generation. In this manner, the higher-order modes generated in a single antenna structure with directional radiation patterns resulting in low spatial correlation in angle space are used as diversity ports in a MIMO system within a compact space. In pattern diversity on the other hand that is slightly different than multimode diversity, orthogonal radiation patterns generated on distinct antennas that are co-located at the phase-centers are generated and used as diversity ports.

In this work, a multimode stacked circular microstrip patch antenna used in a uniform linear array structure (SCP-ULA) for MIMO-OFDM WLAN systems conforming to IEEE 802.11n standard is designed and the associated correlation, ergodic spectral efficiency and compactness with respect to omnidirectional dipole (DP-ULA) and circular microstrip uniform linear arrays (CP-ULA) operating in the dominant TM_{01} mode are analyzed. Section II and Section III is dedicated to the design procedure of stacked circular microstrip antenna for IEEE 802.11n MIMO-OFDM WLAN communication in HFSSv.11 CAD program and the analysis of the marginal and superposition radiation patterns as well as S-parameters and VSWR variations versus frequency respectively. In Section IV, the gain of SCP-ULA with respect to CP-ULA and DP-ULA in terms of spatial/modal correlations, ergodic spectral efficiency and compactness are presented. Finally, Section V concludes the paper.

II.DESIGN OF MULTIMODE STACKED CIRCULAR PATCH (SCP) MICROSTRIP ANTENNA

In the multimode stacked circular microstrip antenna designed for MIMO-OFDM WLAN application, the upper antenna in a stack is excited at the TM_{11} mode and the bottom

978-1-4244-2721-5/09/$25.00 ©2009 IEEE

antenna is excited at the TM_{21} mode to meet the compactness requirements since the radius of a circular microstrip patch antenna scales up with the mode number *m* excited given by [8]:

$$a = \frac{\chi_m \lambda}{2\pi\sqrt{\varepsilon_r}} \quad (1)$$

where χ_m indicates the first zero of the derivative of second kind Bessel function of order m $J_m(x)$ as in Table I.

TABLE I

χ_m FOR DIFFERENT MODES

	TM_{01}	TM_{11}	TM_{21}	TM_{31}	TM_{41}	TM_{51}	TM_{61}
χ_m	3.82	1.84	3.04	4.18	5.29	6.38	7.46

Furthermore, the far-field radiation pattern for a circular microstrip patch antenna excited with *m*th mode is also given by [8]:

$$\vec{E}_m = \frac{e^{-jk_f r}}{r}\left(E_{m,\theta}\vec{\theta} + E_{m,\phi}\vec{\phi}\right) \quad (2)$$

$$E_{m,\theta} = \frac{j^m V_m^0 k_f a}{2}\left[J_{m+1}(z) - J_{m-1}(z)\right]\cos(m(\phi-\phi_0)) \quad (3)$$

$$E_{m,\phi} = -\frac{j^m V_m^0 k_f a}{2}\left[J_{m+1}(z) + J_{m-1}(z)\right]\cos(\theta)\sin(m(\phi-\phi_0)) \quad (4)$$

where $k_f = 2\pi/\lambda$ is the wavenumber, $J_m(x)$ is the Bessel function of second kind of order *m,* a is the patch radius, V_m^0 is the peak input voltage of *m*th mode, ϕ_0 is the reference azimuth angle for the feed of the circular patch, and $z = k_f a \sin(\theta)$. Via these far-field radiation patterns, neglecting elevation spread that is acceptable for indoor propagation environments and assuming the look-direction coincident with broadside is $\theta = \pi/2$, only θ components of the farfield radiation pattern dependent on the azimuth angle ϕ in (3) remains.

The SCP antenna fed by microstrip feed lines designed in HFSSv.11 3D EM design and analysis software is presented in

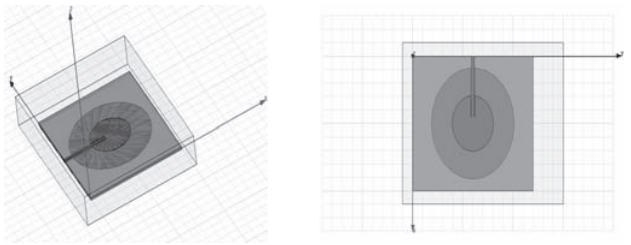

(a) (b)

Fig.1 The side (a) and the top (b) view of the SCP antenna with microstrip feed line in HFSS

Fig. 1. To stay at the proper point of the trade-off between antenna bandwidth improvement and the antenna efficiency decrease/pattern distortion as well as to keep mutual coupling low, the distances between ground and bottom antenna as well as between circular antennas are kept as 0.5 mm.

The theoretical radius of the top and bottom antennas in SCP excited by TM_{11} and TM21 modes via (1) are respectively given by 10.2 mm and 17 mm respectively. However, including the Fringing effect [7], the actual effective radius of the circular patch antenna that is larger than estimated by (1) is given by:

$$a_e = a\left(1 + \frac{2h}{\pi a \varepsilon_r}\left(\ln\left(\frac{a}{2h}\right) + (1{,}41\varepsilon_r + 1{,}77) + \frac{h}{a}(0{,}26\varepsilon_r + 1{,}65)\right)\right)^{1/2} \quad (5)$$

through which the effective radiuses of TM11 and TM21 modes are 10.6 mm and 17.4 mm respectively. To operate both stack elements at the same frequency, the radius of the antenna of TM_{21} mode is set as 20.67 mm by the HFSS while the radius of the antenna operating on TM_{11} mode is used according to the theoretical value of 10.26 mm.

For impedance matching of the SCP antenna at 802.11n upper ISM band WLAN operating frequency of 5.8 GHz, the radiation resistances for both element antennas have to be evaluated first for TM_{11} mode and TM_{21} modes. The real Poynting vector is given by [9]:

$$P + jQ = \frac{1}{2}\int\int_{size}\left(\vec{E}_{ax}\vec{H}_a^{\,*}\right)\hat{z}dxdy \quad (6)$$

and integrating the real part of (6):

$$P_r = \frac{1}{2\eta_0}\int_0^{2\pi}\int_0^{\pi/2}\left(|E_\theta|^2 + |E_\varphi|^2\right)r^2\sin\theta d\theta d\varphi \quad (7)$$

The relation between (7) and the radiation resistance R_r is given by:

$$P_r = \frac{1}{2}G_r(E_0 h)^2 = \frac{1}{2}G_r V_0^2 \quad (8)$$

$$R_r = \frac{1}{G_r} \quad (9)$$

where G_r is the radiation conductance. In this manner, the radiation resistance of elements operating on TM_{11} mode and and TM_{21} mode are obtained as 342.57 Ω and 156.13 Ω respectively(8)-(9). In stack antenna the radiation resistance of TM_{21} mode is further obtained as 131.21 Ω and the radiation resistance of TM_{11} mode is found 315.04 Ω in HFSS.

Antenna input impedances are described by the equations:

$$Z_{in} = R_{in} + jX_{in} \quad (10)$$

$$R_{in} = \frac{1}{G_{in}} \quad (11)$$

$$G_{in} = G_r + G_d + G_c \quad (12)$$

where Z_{in}, is input impedance, R_{in} is input resistance, X_{in} is input reactance, G_{in} is input conductance, G_d is dielectric conductance and G_c is the conductor conductance respectively. Since the antenna patch used in the design is selected as a zero-loss conductor, there exists no conductor resistance. On the other hand, the dielectric conductance value can be calculated via [10] as:

$$G_d = \frac{\varepsilon_{m0}\tan\delta}{4\mu_0 h f_r}\left[(ka_r)^2 - m^2\right] \quad (13)$$

where $\varepsilon_{m0} = 2$ for *m*=0 and $\varepsilon_{m0} = 1$ for $m \neq 0$. The effective loss tangent of the dielectric material with ε_r =2.2 is determined as δ =0.0009. Using these values, the dielectric

conductances for TM_{11} and TM_{21} modes are obtained as G_d=1.4925x10^{-4} and G_d=6.0936x10^{-4} respectively. These values are quite small so that it is rational not to take dielectric conductances into account for G_{in} calculations and to state that the input resistances of the antenna operating at TM_{11} mode is 342.57 Ω, and the input resistance of the antenna operating at TM_{21} mode is 156.13 Ω. To adapt these resistance values to 50 Ω , microstrip feed line width for both elements in stacked antenna are determined as 1.5 mm via the guideline equations in [11] so that both stack elements are matched to 50Ω input resistance.

Antenna reactances calculated via :

$$X_{in} = -jw\mu_0 h\left[\frac{1}{\pi a_e^2 k^2} + \sum_{m=2}^{\infty}\frac{j_0^2 k_{0m}\rho_0}{\pi a^2 j_0^2 k_{0m} a_e (k^2 - k_{0m}^2)} + \frac{2}{\pi}\sum_{m=1}^{\infty}\left(\frac{\sin(n\Delta)}{n\Delta}\right)^2\right] \quad (14)$$

for TM_{11} and TM_{21} modes are -j162.7 Ω and –j107.13Ω respectively. In stack antenna, the evaluation of the reactances of antenna with TM_{21} mode is obtained as j77.316 while that of TM_{11} mode is found j123.25Ω. In this case, optimizing the length of the microstrip feed lines in HFSS, the antenna reactances of TM_{11} mode and TM_{21} mode are minimized to j11.513 Ω and j4.5072 Ω respectively. Consequently, the antenna input impedances are Z_{in1}=45.507+j11.513Ω and Z_{in2}=50.678+j4.5072 Ω for TM_{11} and TM_{21} modes respectively.

III. ANALYSIS OF SCP ANTENNA

The S-parameters versus frequency of the designed SCP antenna are analyzed in Fig. 2 . The resonance of both modes

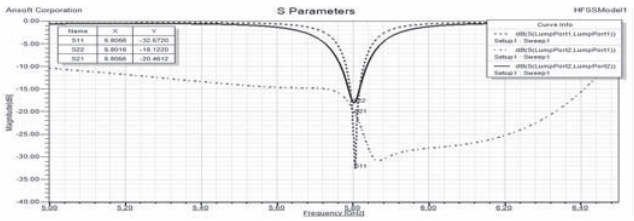

Fig. 2. S-parameters versus frequency of SCP antenna

are achieved around 5.8 GHz that is suitable for MIMO-OFDM WLANs operating in upper ISM band and the operating bandwidth of the SCP antenna is measured around 55 MHz via S_{11} and S_{22} return-loss S-parameters that is sufficiently adequate for IEEE 802.11 WLAN communication which requires 40 MHz bandwidth. Furthermore, the S_{21} mutual-coupling S-parameter in Fig. 2 is well approximately -20 dB within the operating bandwidth around 5.8 GHz letting the omittance of pattern distortion due to coupling effects between the collocated antennas. This fact is also well apparent in Fig. 3 where the the radiation patterns of both modes are presented marginally and in superimposed form. Due to the low mutual coupling achieved, the radiation pattern distortion imposed by TM_{21} mode on TM_{11} mode is negligible in the superimposed radiation pattern in Fig. 3-(c).

The VSWR plots of the SCP antenna for both TM_{11} and TM_{21} modes versus frequency are further presented in Fig. 4. The VSWR values for the TM_{11} and TM_{21} modes at the resonance frequency of 5.8 GHz is measured in HFSS as

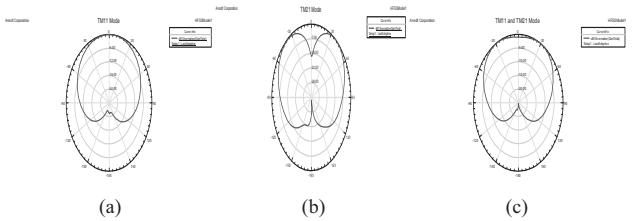

(a) (b) (c)

Fig. 3. Radiation patterns of SCP antenna: (a): TM_{11} alone, (b): TM_{21} alone, (c): TM_{11} and TM_{21} superimposed.

1.0482 and 1.2835 respectively that are very close to the theoretical lower bound of unity validating the reliability of the impedance matching of SCP antenna.

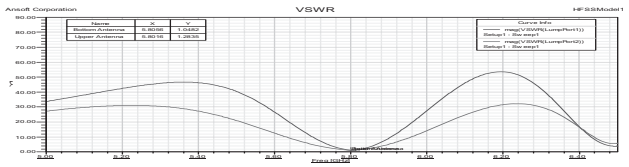

Fig. 4 VSWR plots for SCP antenna.

IV.CORRELATION AND CAPACITY ANALYSIS

To evaluate the achievable gains with SCP antenna used as a uniform linear array (SCP-ULA) for IEEE 802.11 n MIMO-OFDM WLAN communications when employed at access points, modems or end-user terminal equipments, the spatial/modal power correlations of the SCP-ULA is compared with the spatial/modal power correlations of uniform linear arrays of center-fed dipole antennas (DP-ULA) and spatial/modal power correlations of uniform linear arrays of isotropic TM_{01} dominant-mode operating circular patch antennas in Fig. 5 for a statistically-clustered indoor propagation environment with single-cluster of angular spread σ_c^2 and uniformly-distributed mean angle of arrival (AoA) and angle of departure (AoD) with respect to array broadsides. The spatial/modal normalized complex correlation coefficient of all three types of antennas is given by:

$$\rho = \frac{\int_{-\pi}^{\pi} E_1(\phi)E_2^*(\phi)PAS(\phi;\phi_c,\sigma_c^2)\exp\left(-jk_f d(n_2-n_1)\sin(\phi)\right)d\phi}{\sqrt{\int_{-\pi}^{\pi}|E_1(\phi)|^2 PAS(\phi;\phi_c,\sigma_c^2)d\phi}\cdot\sqrt{\int_{-\pi}^{\pi}|E_2(\phi)|^2 PAS(\phi;\phi_c,\sigma_c^2)d\phi}} \quad (15)$$

and the power azimuth spectrum (PAS) $PAS(\phi;\phi_c,\sigma_c^2)$ that defines the distribution of power over the sub-multipath components within a cluster is used as truncated-Laplacian density with mean azimuth angle ϕ_c and angular spread σ_c^2 the form of which is given by [12]:

$$PAS(\phi;\phi_c,\sigma_c^2) = \frac{e^{-\left|\frac{\sqrt{2}(\phi-\phi_c)}{\sigma_c}\right|}}{\sqrt{2}\sigma_c\left(1-e^{-\frac{\sqrt{2}\pi}{\sigma_c}}\right)} \quad (16)$$

that is suitable for indoor propagation environments. The power correlation values that is strictly related to SNR scaling for MIMO channels is then given by $\rho_p = |\rho|^2$ and the power correlation values are averaged over uniformly-distributed mean azimuth angles over ϕ.

The power correlation values of the SCP antenna for all angular spread values and spatial/modal combinations in the densest configuration where stack antennas are nearby in the most compact scenario allowed by the physical radius of the bottom antenna for 4×4 configuration as presented in Fig. 5 are much lower than that of the two nearest antennas spaced at the patch radius of SCP bottom antenna in $\lambda/2$ DP-ULA and CP-ULA which dictates spectral efficiency and transmission quality gains for MIMO spatial-multiplexing.

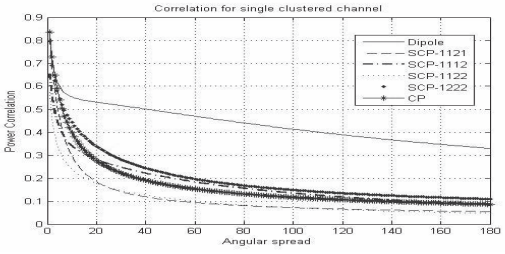

Fig. 5 Power correlation values of DP-ULA, CP-ULA and SCP-ULA

The ergodic spectral efficiencies in bps/Hz of MIMO-OFDM WLAN system with DP-ULA, CP-ULA and SCP-ULA versus angular spread for 2×2 and 4×4 configurations are further presented in Fig. 6 over single-cluster Kroenecker-model NLOS Rayleigh fading channel via [13]:

$$\eta = E\left\{\frac{1}{N_c}\sum_{i=1}^{N_c}\log_2\left(\det\left(\mathbf{I}_N+\frac{SNR}{M}\mathbf{H}_c\mathbf{H}_c^{\,H}\right)\right)\right\} \quad (16)$$

where the correlated channel matrix $\mathbf{H}_c$ has the Kroenecker form [14]; $\mathbf{H}_c=\mathbf{R}_{RX}^{1/2}\mathbf{H}_w\mathbf{R}_{TX}^{1/2}$, in terms of the receive and transmit normalized correlation matrices $\mathbf{R}_{RX}$ and $\mathbf{R}_{TX}$, and the elementwise-independent $N\times M$ Wishart–type random matrix $\mathbf{H}_w$ with elements distributed as $CN(0,1)$. For both 2×2 and 4×4 configurations, the SCP-ULA has much higher spectral efficiency than DP-ULA and slightly higher spectral efficiency than CP-ULA Most importantly, these lower correlation and higher spectral efficiency gains are achieved at %33.3 and %49.9 denser space with SCP-ULA with respect to DP-ULA and CP-ULA for 4x4 configuration as tabulated in Table II. Furthermore, based on the spectral efficiency results presented in Fig.6, data rates achievable with SCP-ULA conforming to IEEE 802.11n standards with 40MHz bandwidth for 2x2 and 4x4 array configurations are 164 Mbps and 324 Mbps respectively for high angular spreads that are much higher than standard 125 Mbps data rate achievable with SISO 802.11 a/b/g WLAN systems.

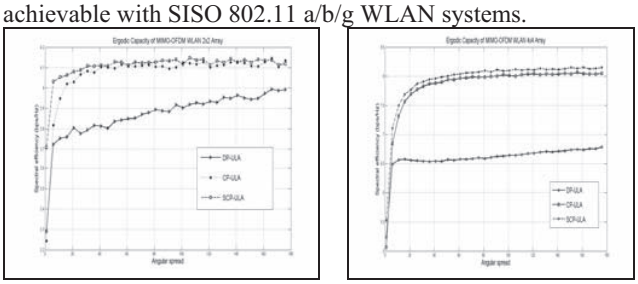

(a) (b)

Fig. 6 Ergodic spectral efficiency of MIMO-OFDM WLAN over Kroenecker-based statistically-clustered single-cluster NLOS Rayleigh fading channel with DP-ULA, CP-ULA and SCP-ULA versus angular spread at SNR=10 dB, (a): 2x2, (b): 4x4

V.CONCLUSIONS

In this paper, the design and analysis of a stacked antenna comprised of multimode circular microstrip patch antennas for deployment in access points, modems and end-user terminal equipments of IEEE 802.11n compliant MIMO-OFDM WLAN systems is presented. The lower correlation, higher spectral efficiency and physical compactness of the SCP-ULA compared to the conventional uniform linear arrays formed of center-fed dipole elements or single circular microstrip patch elements represents SCP-ULA as a promising solution for use in the spatially-compact communication equipments of next-generation high-speed WLAN systems.

TABLE II

COMPACTNESS GAIN OF SCP-ULA W.R.T. CP-ULA AND DP-ULA

(TYPE)/(NXM)	2X2 (%)	4X4 (%)
DP-ULA	0	33.3
CP-ULA	49.7	49.9

ACKNOWLEDGMENT

This work is supported by Turkish Scientific and Technological Research Council (TÜBİTAK) R&D Project EEEAG-108E025.

REFERENCES

[1] I. E. Telatar. Capacity of Multi-antenna Gaussian Channels. European Trans. on Telecomm., vol. 10, pp. 585–596, November 1999.

[2] A. Forenza and R. W. Heath. Benefit of Pattern Diversity via Two-Element Array of Circular Patch Antennas in Indoor Clustered MIMO Channels. *IEEE Transactions on Communications*, vol. 54, no. 5, pp. 943-954, May 2006.

[3] Matilde Sanchez-Fernandez, Eva Rajo-Iglesias, Oscar Quevedo-Teruel, M. Luz Pablo-Gonzalez. Spectral Efficiency in MIMO Systems Using Space and Pattern Diversities Under Compactness Constraints. *IEEE Transactions on Vehicular Technology*, vol. 57, no.3, pp. 1637-1645, May 2008.

[4] T. Svantesson. Correlation and Channel Capacity of MIMO Systems Employing Multimode Antennas. *IEEE Transactions on Vehicular Technology,* vol. 51, no. 6, pp. 1304-1312, November 2002.

[5] A. Mukherjee and Hyuck M. Kwon. Compact Multi-user Wideband MIMO System Using Multiple-Mode Microstrip Antennas. Proceedings of *Vehicular Technology Conference Spring- 2007*, pp. 584-588, April 2007.

[6] C. Waldschmidt, C. Kuhnert, S. Schulteis, and W. Wiesbeck, Compact MIMO-Arrays Based on Polarization-Diversity. *Proeedings.of IEEE Antennas and Propagaion. Symp*., vol. 2, pp. 499-502, June 2003.

[7] T. Svantesson. On the Capacity and Correlation of Multi-Antenna Systems Employing Multiple Polarizations. *Proceedings of IEEE Antennas and Propagation Symposium,* vol. 3, pp. 202-205*, June 2002*.

[8] R. G. Vaughan. Two-Port Higher Mode Circular Microstrip Antennas. *IEEE Transactions on Antennas and Propagation,* vol. 36, no. 3, pp. 309-321, March 1988.

[9] R. Garg, P. Bhartia, I. Bahl. *Microstrip Antenna Design Handbook*. Artech House, 2001.

[10] C.A. Balanis. *Antenna Theory: Analysis and Design*, 2nd ed. United States of America, John Wiley&Sons Inc., 1997.

[11] I. Bahl. *Lumped Elements for RF and Microwave Circuits*. Boston, Artech House, 2003.

[12] TGn Channel Models. IEEE 802.11-03/940r4, May 2004.

[13] A. van Zelst, R. Van Nee and G. A. Awater. Space-Division Multiplexing for OFDM Systems. IEEE Vehicular Technology Conference – Spring, vol.2, pp. 1070-1074, May 2000.

[14] C. N. Chuah, J. M. Kahn and D. N. C. Tse. Capacity of Multiantenna Array Systems in Indoor Wireless Environments. Proceedings of GLOBECOM'98, vol. 4, pp. 1894-1899, Sidney, Australia, November 1998.